

Article

Assessing the Impact of Spatiotemporal Land Cover Changes on the Urban Heat Islands in Developing Cities with Landsat Data: A Case Study in Zhanjiang

Yutian Hu ¹, Hongye Li ¹ , Muhammad Amir Siddique ² and Dongyun Liu ^{1,*}

¹ School of Landscape Architecture, Beijing Forestry University, Beijing 100107, China; hyt886@bjfu.edu.cn (Y.H.); lhy777@bjfu.edu.cn (H.L.)

² School of Architecture, Tianjin University, Tianjin 300272, China; amir@tju.edu.cn

* Correspondence: dongyun_laurstudio@bjfu.edu.cn

Abstract: Land cover changes (LCCs) due to urbanization cause urban heat islands (UHIs), significantly affecting land surface temperature (LST) through spatiotemporal changes in compositions, parameters, and patterns. Land cover and LST have been studied in various cities; however, indicative research into heterogeneous LCC's impact on LST in less-developed cities remains incomplete. This study analyzed new Landsat images of Zhanjiang, taken from 2004 to 2022, to determine the impact of three LCC indicators (compositions, parameters, and patterns) on LSTs. The urban thermal field variance index (UTFVI) was used to describe the distribution and variation in LST. We also quantified the cooling or warming benefits of various LCCs. The results indicate that the average temperature in the land urban heat island (SUHI) area rose to 30.6 °C. The average temperature of the SUHI was 3.32 °C higher than that of the non-SUHI area, showing the characteristic of shifting to counties and multi-core development. The LST increases by 0.37–0.67 °C with an increase of 0.1 in the normalized difference building index (NDBI), which is greater than the cooling benefit of the normalized difference of vegetation index (NDVI). The impact of landscape pattern indices on impervious surfaces and water is higher than that on vegetation and cropland, with a rising influence on impervious surfaces and a decreasing impact on water. The predominant cooling patches are vegetation and water, while large areas of impervious surface and cropland aggravate UHIs for industrial and agricultural activities. These findings are intended to guide future urban layouts and planning in less-developed cities, with thermal climate mitigation as a guiding principle.

Keywords: urban heat island; Landsat data; land cover changes; landscape pattern; UTFVI



Citation: Hu, Y.; Li, H.; Amir Siddique, M.; Liu, D. Assessing the Impact of Spatiotemporal Land Cover Changes on the Urban Heat Islands in Developing Cities with Landsat Data: A Case Study in Zhanjiang. *Atmosphere* **2023**, *14*, 1716. <https://doi.org/10.3390/atmos14121716>

Academic Editors: Francesca Despini and Sofia Costanzini

Received: 28 September 2023

Revised: 12 November 2023

Accepted: 16 November 2023

Published: 22 November 2023



Copyright: © 2023 by the authors. Licensee MDPI, Basel, Switzerland. This article is an open access article distributed under the terms and conditions of the Creative Commons Attribution (CC BY) license (<https://creativecommons.org/licenses/by/4.0/>).

1. Introduction

As urbanization accelerates, artificial impermeable surfaces gradually replace permeable natural landscape surfaces [1], exacerbating the urban thermal environment. This is because the use of urban elements, such as concrete, asphalt pavements [2], and building materials, continues to rise, increasing sensible heat fluxes and affecting the degree of absorption of solar radiation by the ground surface while also altering albedo and evaporation rate [3,4]. Due to this effect, densely populated urban areas have higher LSTs than suburban areas [5]. Water quality, surface temperature, and environmental quality can be affected by UHIs, as well as excess energy consumption [6]. Moreover, they can adversely affect residents' respiratory and cardiovascular systems and cause negative depression [7–9]. Increased natural landscape surfaces can often mitigate UHIs compared to impervious surfaces. This is especially true for green spaces that can produce shadows capable of covering the ground surface [10], create a cold island effect through evapotranspiration and emissivity, and lower thermal inertia [11]. To study environmental change, it is becoming increasingly important to analyze the impact of urban land cover changes (LCCs) on the thermal environment [12].

Land cover composition and parameters exert a profound effect on LST, especially in cities characterized by urban sprawl, population expansion, and rapidly growing economies [13]. Indeed, the difference in land cover composition affects the change in land parameters as well. Some studies quantify the correlation between underlying surface parameters and LST. For example, the normalized difference vegetation index (NDVI) and the normalized difference building index (NDBI) were used to explore proper functioning with LST at different square scales in Beijing. It was concluded that the relationships between NDVI, NDBI, and LST were significant but that their correlation was nonlinear [14]. Taking Kunming as an example, NDVI, NDBI, and the normalized difference water index (MNDWI) were used to explore the correlation between land surface characteristics and LST and analyze the joint cooling benefits shared between the indices. It was pointed out that NDVI and MNDWI were linearly correlated with LST and that the combination of the two was the best indicator of LST relative to the others [15]. Similar research methods have been used and progress made in mega-cities such as Shanghai, Guangzhou, Wuhan, and Nanjing, with relevant studies reaching the common conclusion that, in urban areas, elevated NDVI promotes a decreased LST and that elevated NDBI can increase LST [16–19]. In terms of land cover composition, cities such as Shanghai, Zhengzhou, and Chengdu have demonstrated that impervious surfaces or buildings contribute more to the heating of houses and buildings than natural surfaces [20–22]. However, the generalizability of these findings to China's slower-growing cities still needs to be examined in more comprehensive studies. As mentioned in the outline of the 14th Five-Year Plan, the main tasks and initiatives to improve the new urbanization strategy include improving the spatial pattern of urbanization and preserving a reasonable ecological safety distance between cities. To ensure the coexistence of urban economic development and a green, livable environment, the future land use planning of developing cities needs to be given sufficient attention.

Land cover contributes thermally to LST. This is not only because of its composition but also because of its configuration and pattern [23]. Related studies have shown that the cooling capacity of water bodies and green space landscapes is influenced by spatial configuration [24,25] and that the aggregation of blue-green patches combined with the dispersion of impervious surfaces can effectively mitigate UHIs [26,27]. Land cover configuration is usually quantified using landscape pattern indices, such as the Shannon diversity index (SHDI), the contagion index (CONTAG), the landscape division index (DIVISION), and the landscape shape index (LSI), to explore the correlation between land cover configuration and LST [28]. In Beijing, only suburban areas were significantly correlated with land cover configuration and LST. At the same time, a survey in Fuzhou demonstrated that type-level indicators—aggregation index (AI), average patch area (AREA_MN), largest patch index (LPI), and percentage of landscape (PLAND)—of impervious surfaces were significantly and positively correlated with LST, while the opposite was true for vegetation and water bodies [29]. Landscape pattern indices with different categories and levels of land cover exert varying effects on LST. Meanwhile, the influence of landscape pattern on LST is characterized by density [30], scale [31,32], urban–rural gradient difference, etc. LST varies across cities with different latitudes and longitudes depending on landscape configuration [33,34]. Furthermore, past studies focused more on landscape configuration indicators at the landscape level than at the level of type [35]. Hence, it is essential to evaluate the spatiotemporal dynamics of the relationship between land cover types and thermal environments in other developing cities.

Analysis of the spatiotemporal differences generated by changes in land cover types and their correlation with LST is conducive to the derivation of appropriate landscape configurations of land cover types. Therefore, this study takes Zhanjiang as the research area and aims to: (1) investigate the spatiotemporal differences in LST; (2) determine the land cover composition and parameters; (3) conduct a correlation analysis of the thermal effects of different types of land cover at the parametric and pattern-related levels; and (4) make reasonable suggestions for the future land use planning and landscape

configuration of Zhanjiang, with the healthy development of the thermal environment as the research orientation.

2. Materials and Methods

2.1. Study Area

Zhanjiang is a city in Guangdong Province, lying in the southern part of China at latitudes of 20°13' N to 21°57' N and longitudes of 109°40' E to 110°58' E. It has a tropical and subtropical monsoon climate regulated by the ocean climate throughout the year, causing an annual average temperature of 23 °C. Most of the land consists of peninsulas and islands, covered by plains and terraces with an average elevation of 24 m. Zhanjiang is an essential modern port and industrial city on the southeast coast. At the end of 2021, Zhanjiang had a permanent population of 7,030,900, including 3,266,600 people in urban areas, representing approximately 46.46% of the population. The study area is 13,263 square kilometers, including four municipal districts and two counties, with three county-level cities under escrow (Figure 1).

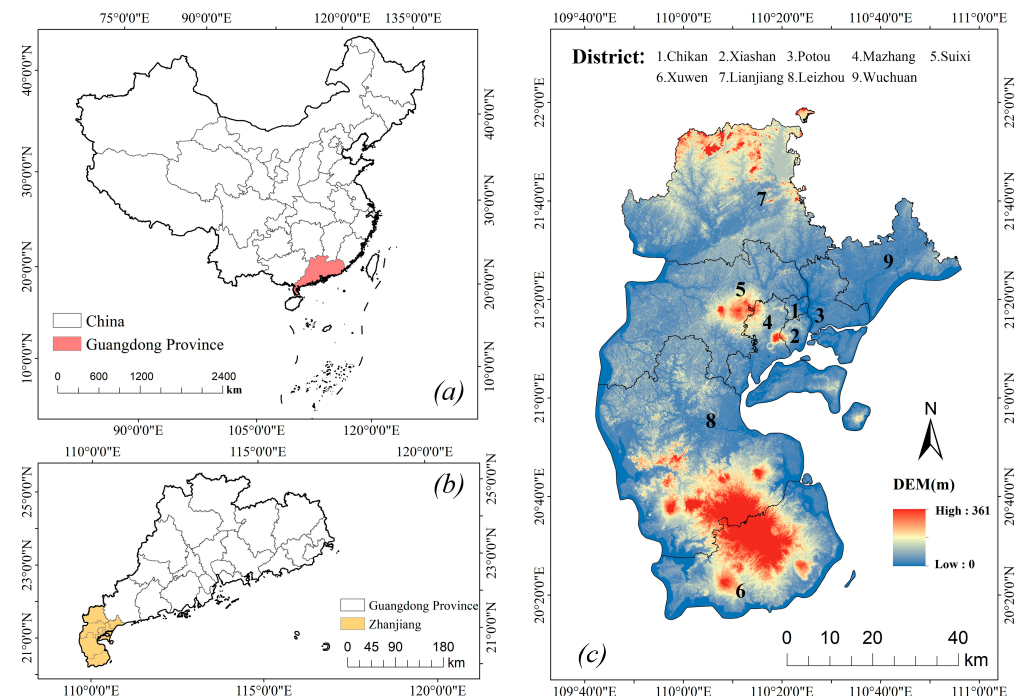


Figure 1. Study area: Zhanjiang and its geographical location (a–c).

2.2. Preprocessing of Spatial Data

The study used the Landsat5 data taken on 18 November 2004, Landsat8 data extracted on 26 October 2013, and Landsat9 data captured on 11 October 2022 from the USGS Earth Explorer user interface (<https://earthexplorer.usgs.gov/>). Satellite images were time-converted into Eastern Standard Time (UTC/GMT +8:00) for atmospheric correction (Table 1). Before processing the data, ortho grinding and calibration were performed in ENVI 5.3 using the “Radiometric Calibration” tool, and atmospheric correction was performed using the “FLAASH Atmospheric Correction” tool.

Table 1. Details of the temporal images.

Satellite Type	Date	Observation Time (UTC/GMT+08:00)	Cloud Cover
Landsat5	18 November 2004	10:49:57	0.00%
Landsat8	26 October 2013	11:06:37	2.48%
Landsat9	11 October 2022	11:05:16	0.17%

2.3. Spatiotemporal Analysis

The research analysis framework is shown in Figure 2. First, we selected the spatiotemporal data for the supervised classification of land use compositions and used Fragstats v4.2.1 to calculate the landscape pattern. Second, LSTs were obtained by surface-temperature inversion when the land surface parameters NDVI and NDBI were calculated. Finally, the data obtained were analyzed using the least-squares model in order to establish the main factors affecting the intensification of the surface thermal environment in Zhanjiang City.

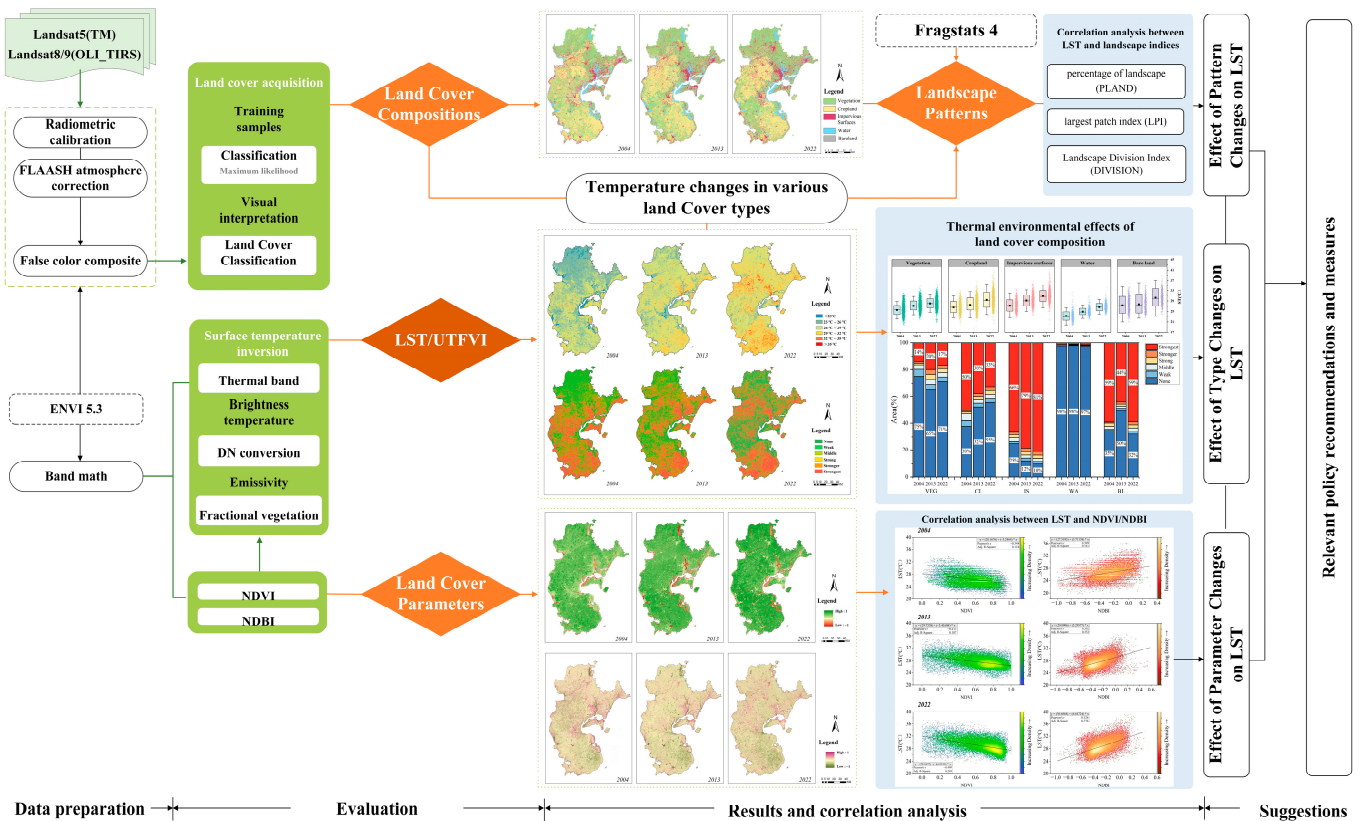


Figure 2. Research framework.

2.3.1. Land Use Cover Classification

Combined with the characteristics of Zhanjiang, the land cover was divided into vegetation, cropland, impervious surfaces, water, and bare land (Table 2). The maximum likelihood method in supervised classification was used to extract information on the land cover types from remote sensing images. Due to the severe mixing of cropland and vegetation image elements, the image elements were manually modified after supervised classification combined with visual interpretation. Finally, clump classes and majority/minority analysis tools were used in ENVI5.3 to aggregate small patches and reduce noise.

Table 2. Land cover classification types in the study area.

Classifications	Abbreviations	Description
Vegetation	VEG	Forest, grassland, and urban and rural tree plantation
Cropland	CL	Agricultural plantation
Impervious surfaces	IS	Built-up areas including buildings and roads
Water	WA	Lake, pond, river, reservoir, and part of the sea
Bare land	BL	Bare soil or rocks, mudflat, and other unbuilt zones

The confusion matrix was used to classify accuracy and the kappa coefficient in ENVI 5.3. Four indicators were generated from the overall evaluation of EVVI5.3: user accuracy, producer accuracy, overall accuracy, and the kappa coefficient. Compared to other metrics, the kappa coefficient is a measure of consistency based on the difference between actual and opportunity agreement in an error matrix. The kappa coefficient was defined by Equation (1). In each image, 450 test points were used to determine accuracy.

$$Kappa\ coefficient = \frac{N \sum_{k=1}^m X_{kk} - \sum_{k=1}^m (X_{k+} * X_{+k})}{N^2 - \sum_{k=1}^m (X_{k+} * X_{+k})}, \tag{1}$$

where, N = total number of pixels; m = number of rows in matrix; X_{kk} = number of observations in row k and column k ; and X_{k+} and X_{+k} are the marginals for row k and column k , respectively.

2.3.2. Landscape Pattern Calculation

To demonstrate the impact of various landscapes on the LST, the percentage of landscape (PLAND), maximum patch indices (LPI), and landscape division index (DIVISION) were selected from the type level (Table 3). Landscape pattern indices were visualized in Fragstats 4.2 using the moving window method. Regarding the size choice of the moving window, some researchers opted for 240 m and 450 m [11,24]. Some studies believed that the spatial resolution of 500 m could reflect the regional landscape composition for an area of about 2000 km² [36]. When the moving window is 720, all the study coefficients that characterize the landscape components reach a maximum; conversely, at resolutions coarser than 720 m, most coefficients are insignificant [37]. Considering the research results and the area size of Zhanjiang, a grid of 720 m × 720 m was selected as the size of the moving window.

Table 3. Relevant descriptions of landscape pattern indices.

Metric	Formula	Description	Range
Percentage of landscape (PLAND)	$PLAND = P_i = \frac{\sum_{j=1}^n a_{ij}}{A} (100)$	The percentage of different types of landscape in the unit window	$0 < PLAND \leq 100$
Largest patch index (LPI)	$LPI = \frac{\max(a_{ij})}{A} (100)$	The proportion of the largest plaque in the landscape	$0 < LPI \leq 100$
Landscape division index (DIVISION)	$DIVISION = [1 - \sum_{j=1}^n (\frac{a_{ij}}{A})^2]$	Reflects the degree of separation of patches in the landscape	$0 \leq DIVISION < 1$

Note: P_i = proportion of the landscape occupied by patch type (class) i ; a_{ij} = area (m²) of patch ij ; A = total landscape area (m²).

2.3.3. Calculation of Land Use Indices (NDVI and NDBI)

The normalized difference vegetation index (NDVI) was calculated using the near-infrared band (NIR) and red-light band (RED). The normalized difference vegetation index (NDBI) calculations were performed using the near-infrared band (NIR) and mid-infrared band 1 (SWIR-1). NDVI and NDBI values range from [−1, +1].

$$NDVI = (B_{NIR} - B_{RED}) / (B_{NIR} + B_{RED}), \tag{2}$$

$$NDBI = (B_{SWIR1} - B_{NIR}) / (B_{SWIR1} + B_{NIR}), \tag{3}$$

2.3.4. Land Surface Temperature (LST)

The inversion calculations were performed in ENVI5.3. The radiative transfer equation method was used for surface information acquisition [38]. The steps below can be followed to obtain the LST (Table 4).

Table 4. Step for Land surface temperature (LST) acquisition.

Step	Process Name	Formula	References
1	Spectral radiance (SR)	$L_{\lambda 1} = 209.831 + 0.834DN - 0.00133DN^2$ $L_{\lambda 2} = 0.0003342 \times DN + 0.1$	[39–41]
2	Fractional vegetation (Fv)	$P_v = (NDVI - NDVI_s)/(NDVI_v - NDVI_s)$	[42]
3	Surface emissivity (ϵ)	$\epsilon = 0.004 P_v + 0.986$	[37,42]
4	Brightness temperature (TB)	$T_b = ([L_{\lambda} - L_u - t \times (1 - \epsilon) L_d]) / (t \times \epsilon)$	[43]
5	Land surface temperature (LST)	$LST = K_2 / \ln(K_1 / T_s + 1) - 273$	[43,44]

Where DN is the digital number, which represents the pixel brightness value of the remote sensing image; $\lambda 1$ and $\lambda 2$ are the effective wavelength in Landsat 5 and Landsat 8 data, respectively; t is the atmospheric transmittance; and L_u and L_d are the atmospheric upward and downward thermal radiation intensities, respectively, obtained in NASA’s atmospheric correction parameter calculator (<https://atmcorr.gsfc.nasa.gov>). $NDVI_v$ stands for NDVI in the vegetation zone, while $NDVI_s$ signifies NDVI in a completely bare area.

2.3.5. Estimation of UTFVI

To standardize the results for multi-temporal comparison, we used a standardized equation based on LST, which presents the thermal environment scenario called urban thermal field variance index (UTFVI), calculated using Equation (4) [45]:

$$UTFVI = LST_{\text{pixel}} / LST_{\text{mean}} - 1, \tag{4}$$

In Equation (4), LST_{mean} is the mean LST of the total area, and LST_{pixel} is the actual temperature value for each pixel. The results were graded to describe the land urban heat island (SUHI) phenomenon (Table 5). For each pixel, UTFVI greater than 0 means that the temperature is higher than the average LST of the study area, defined as a SUHI region; less than 0 means that the LST is lower than the average LST, defined as a non-SUHI region [45].

Table 5. Urban thermal field variance index (UTFVI) classification.

UTFVI Value	SUHI Degree
<0	None
0–0.005	Weak
0.005–0.010	Middle
0.010–0.015	Strong
0.015–0.020	Stronger
>0.020	Strongest

2.4. Statistical Analysis

In this study, the ordinary least-squares model (OLS) was used to evaluate the correlation between LST and land indices. Depending on the normality of the data, linear regression was used to determine the influence of each index on the change in LST.

3. Results

3.1. Spatiotemporal Change Analysis

3.1.1. LUCC Information

Maps of land use cover changes (LUCC) were spatially prepared for the years 2004, 2013, and 2022 (Figure 3A). Statistics for LUCC from 2004 to 2022 are shown in Table 6. From 2004 to 2013, the most significant increase in the LUCC was for vegetation (VEG), with a total increase of 437.5 km². There was 340.4 km² of bare land (BL) invested in the construction. Cropland (CL) was the most significant type seeing area change except for BL, with a total reduction of about 279 km². Water (WA) saw an increase of 113.4 km², which was higher than that of the impervious surfaces (IS, 68.5 km²). From 2013 to 2022, CL decreased by 226.4 km², which was the most significant alteration. The increase in the IS was second (222.3 km²) only to the change in the CL. There was a decrease of 137.2 km² in VEG, whereas BL had an increase of 72.7 km² as well as an increase of 68.5 km² in WA.

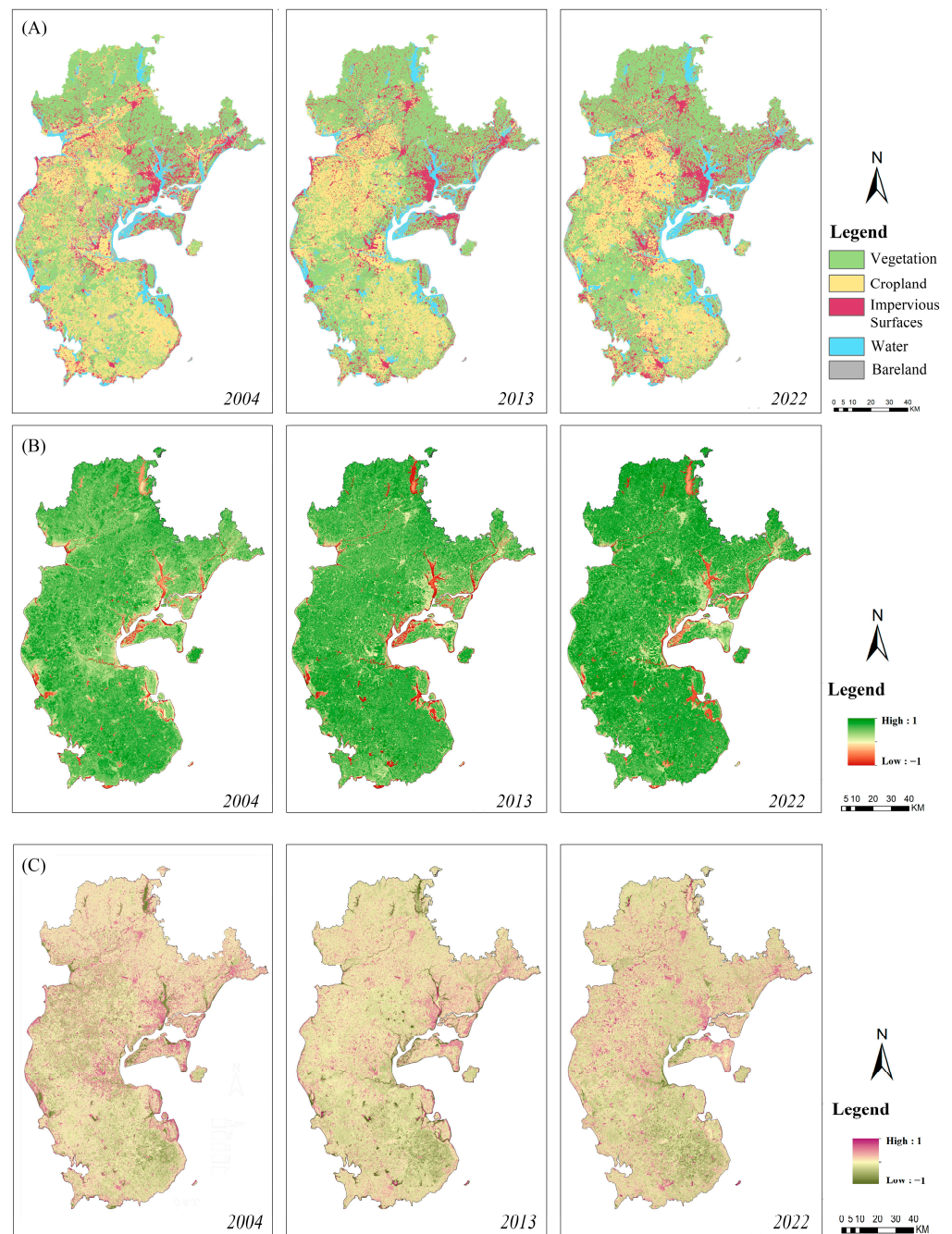


Figure 3. (A) Land use cover changes (LUCC); (B) Normalized difference vegetation index (NDVI); (C) Normalized difference building index (NDBI).

Table 6. Statistics for LUCC from 2004 to 2022.

Landscape Classification	2004		2013		2022	
	Area/km ²	Percentage/%	Area/km ²	Percentage/%	Area/km ²	Percentage/%
Vegetation	5382.521	41.98%	5820.025	45.39%	5682.905	44.32%
Cropland	4381.719	34.17%	4102.721	32.00%	3876.355	30.23%
Impervious surfaces	1587.879	12.38%	1656.388	12.92%	1878.679	14.65%
Water	782.952	6.11%	896.382	6.99%	964.8711	7.53%
Bare land	686.532	5.35%	346.0887	2.70%	418.7943	3.27%

The results of the evaluation of the computational accuracy of classified imagery in 2004, 2013, and 2022 are shown in Tables 7–9. The overall classification accuracies were 90.22%, 91.56%, and 93.11% for 2004, 2013, and 2022, respectively, and the kappa coefficient values were 0.88, 0.89, and 0.91 for 2004, 2013, and 2022, respectively, meeting the minimum level of accuracy for identifying land use and land cover categories from remote sensor data [46].

Table 7. Accuracy assessment result of landscape classification—2004.

Landscape Classification	Reference Totals	Classified Totals	No. Correct	Producer's Accuracy (%)	User's Accuracy (%)	Overall Accuracy (%)	Kappa Score
Vegetation	100	104	88	88.00%	84.62%	90.22%	0.88
Cropland	100	94	84	84.00%	89.36%		
Impervious surfaces	100	107	95	95.00%	88.79%		
Water	100	100	98	98.00%	98.00%		
Bare land	50	45	41	82.00%	91.11%		
Total	450	450	406				

Table 8. Accuracy assessment result of landscape classification—2013.

Landscape Classification	Reference Totals	Classified Totals	No. Correct	Producer's Accuracy (%)	User's Accuracy (%)	Overall Accuracy (%)	Kappa Score
Vegetation	100	109	92	92.00%	84.40%	91.56%	0.89
Cropland	100	104	88	88.00%	84.62%		
Impervious surfaces	100	99	94	94.00%	94.95%		
Water	100	97	97	97.00%	100.00%		
Bare land	50	41	41	82.00%	100.00%		
Total	450	450	412				

Table 9. Accuracy assessment result of landscape classification—2022.

Landscape Classification	Reference Totals	Classified Totals	No. Correct	Producer's Accuracy (%)	User's Accuracy (%)	Overall Accuracy (%)	Kappa Score
Vegetation	100	103	91	91.00%	88.35%	93.11%	0.91
Cropland	100	98	90	90.00%	91.84%		
Impervious surfaces	100	105	97	97.00%	92.38%		
Water	100	101	99	99.00%	98.02%		
Bare land	50	43	42	84.00%	97.67%		
Total	450	450	406				

3.1.2. NDVI and NDBI

The spatiotemporal distributions of NDVI and NDBI in Zhanjiang from 2004 to 2022 are shown in Figure 3B,C. The high-level NDVI showed a trend toward expanding the range and increasing value. In 2004, the NDBI index had scattered high values in regions excluding Xuwen County. However, in 2013 and 2022, the high-value areas were mainly concentrated in the core areas of the central and county-level cities.

3.1.3. Land Surface Temperature (LST)

The distributions of surface temperature in Zhanjiang in 2004, 2013, and 2022 are shown in Figure 4A. The average surface temperature in Zhanjiang was 26.07 °C in 2004, 27.36 °C in 2013, and 28.78 °C in 2022. The area of each type of temperature classification is shown in Table 10. The area below 23 °C decreased by 537.61 km² and 48.25 km², and similarly, the area below 23–26 °C decreased by 3322.34 km² and 1880.12 km² in 2013 and 2022, respectively. The area of the 29–32 °C area increased in 2013 and decreased in 2022. For 29–32 °C, 32–35 °C, and >35 °C, the corresponding areas were increased significantly.

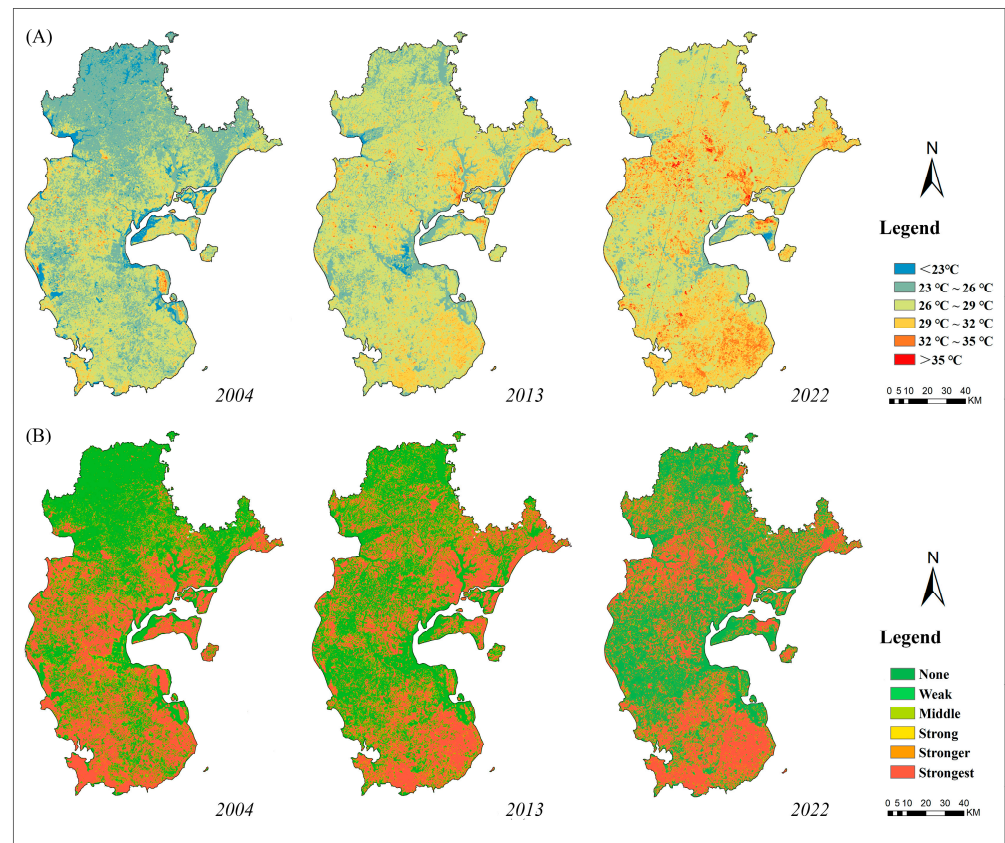


Figure 4. (A) Land surface temperature (LST); (B) Urban thermal field variance index (UTFVI) of Zhanjiang, 2004–2022, at 9-year intervals.

Table 10. Distribution of LST in Zhanjiang, 2004–2022.

LST Grade	2004		2013		2022	
	Area/km ²	Percentage/%	Area/km ²	Percentage/%	Area/km ²	Percentage/%
<23 °C	608.15	47.43%	70.54	0.55%	22.29	0.17%
23–26 °C	5962.59	46.50%	2640.25	20.59%	760.13	5.93%
26–29 °C	5335.51	41.61%	7669.87	59.81%	6682.78	52.11%
29–32 °C	826.90	6.45%	2243.45	17.50%	4309.27	33.61%
32–35 °C	85.44	0.67%	185.52	1.45%	947.15	7.39%
>35 °C	4.50	0.04%	13.46	0.10%	101.46	0.79%

3.1.4. Urban Thermal Field Variance Index (UTFVI)

The spatial distribution of the urban thermal field variance index (UTFVI) in Zhanjiang for 2004, 2013, and 2022 is shown in Figure 4B. Statistical data are shown in Table 11. The area with the ‘None’ grade was 6649.85 km² in 2004, and increased by 89.69 km² and 128.07 km² in 2013 and 2022, respectively. The ‘Weak’ and ‘Middle’ grades showed downward trends year on year. The grades of ‘Strong’ and ‘Stronger’ rose in 2013 and declined in 2022. Conversely, the grade of ‘Strongest’ dropped by 252.54 km² in 2013 and recovered by 65.07 km² in 2022. For spatial distribution, the urban thermal field generally showed a trend of expansion to the north and northwest.

Urban heat intensity denotes the difference in average temperature between land urban heat islands (SUHI) and non-SUHI areas. The temperature difference between SUHI and non-SUHI areas was high, and the average temperature differences between the two were 2.99 °C, 2.91 °C, and 3.32 °C in 2004, 2013, and 2022, respectively (indicated in Figure 5).

Table 11. Distribution of UTFVI in Zhanjiang, 2004–2022.

UTFVI Grade	2004		2013		2022	
	Area/km ²	Percentage/%	Area/km ²	Percentage/%	Area/km ²	Percentage/%
None	6649.85	51.86%	6739.54	52.56%	6867.61	53.56%
Weak	474.91	3.71%	379.97	2.96%	332.12	2.59%
Middle	494.71	3.86%	367.58	2.87%	322.27	2.51%
Strong	170.84	1.33%	356.26	2.78%	306.83	2.39%
Stronger	143.01	1.11%	342.52	2.67%	291.96	2.28%
Strongest	4889.76	38.13%	4637.22	36.16%	4702.29	36.67%

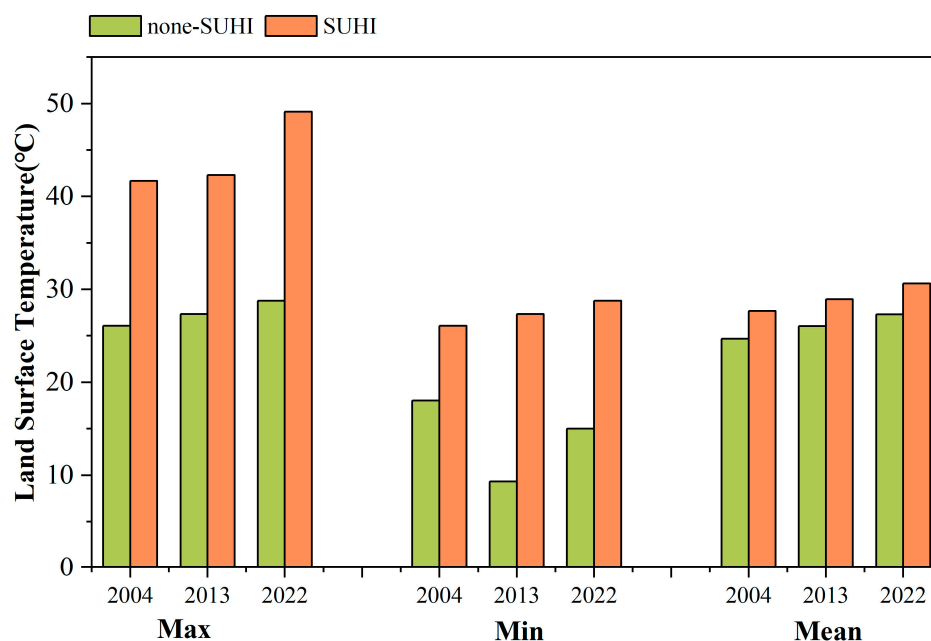


Figure 5. Temperature statistics for SUHI and non-SUHI areas.

3.2. Correlation Analysis

3.2.1. NDVI, NDBI, and LST

Water bodies are cold land types, but at the same time, lack vegetation. To avoid the interference of water bodies, we use the portion of a water body in the land cover map as a mask to exclude this part of the NDVI (Figure 6). NDVI and NDBI for different years passed the significance test ($p < 0.01$). The NDVI was negatively correlated with the LST, while the NDBI was significantly and positively correlated with the LST. The correlation coefficient of NDVI changed from -0.344 to -0.499 , while NDBI rose from 0.399 to 0.526 , tentatively indicating that the influence of land cover parameters on LST rose from 2004 to 2022. The average of both NDVI and NDBI increased, except for the NDBI of 2004.

For every 0.1 increase in the NDVI in 2004, the overall LST fell by approximately $0.32\text{ }^{\circ}\text{C}$. Additionally, by 2022, it was reduced by about $0.47\text{ }^{\circ}\text{C}$, marking an increase of approximately 46.9%. The overall LST increased by $0.38\text{ }^{\circ}\text{C}$ for every 0.1 increase in the NDBI in 2004 and by $0.67\text{ }^{\circ}\text{C}$ for the same rises in 2022, with gains of 76.3% and 29.4% higher than the corresponding increases in NDVI.

3.2.2. Landscape Pattern Indices and LST

The correlation analysis between the landscape pattern and LST was conducted, and three landscape indices, corresponding to VEG, CL, IS, and WA, passed the significance test ($p < 0.01$). The results are shown in Figure 7. Overall, the correlation coefficients showed that PLAND and LPI of VEG and WA were negatively correlated with LST, while

DIVISION showed a positive relationship. PLAND and LPI of CL and IS were positively correlated with LST, while DIVISION revealed a negative relationship. This meant that VEG and WA were the main contributors to UHI mitigation. However, for CL and IS, the above effect was the opposite. Meanwhile, the correlation coefficients of both WA and IS were higher than those of CL and VEG. The absolute values of correlation of VEG in three indicators were all rising, while the opposite was true for WA, indicating that the role of VEG was gradually stronger.

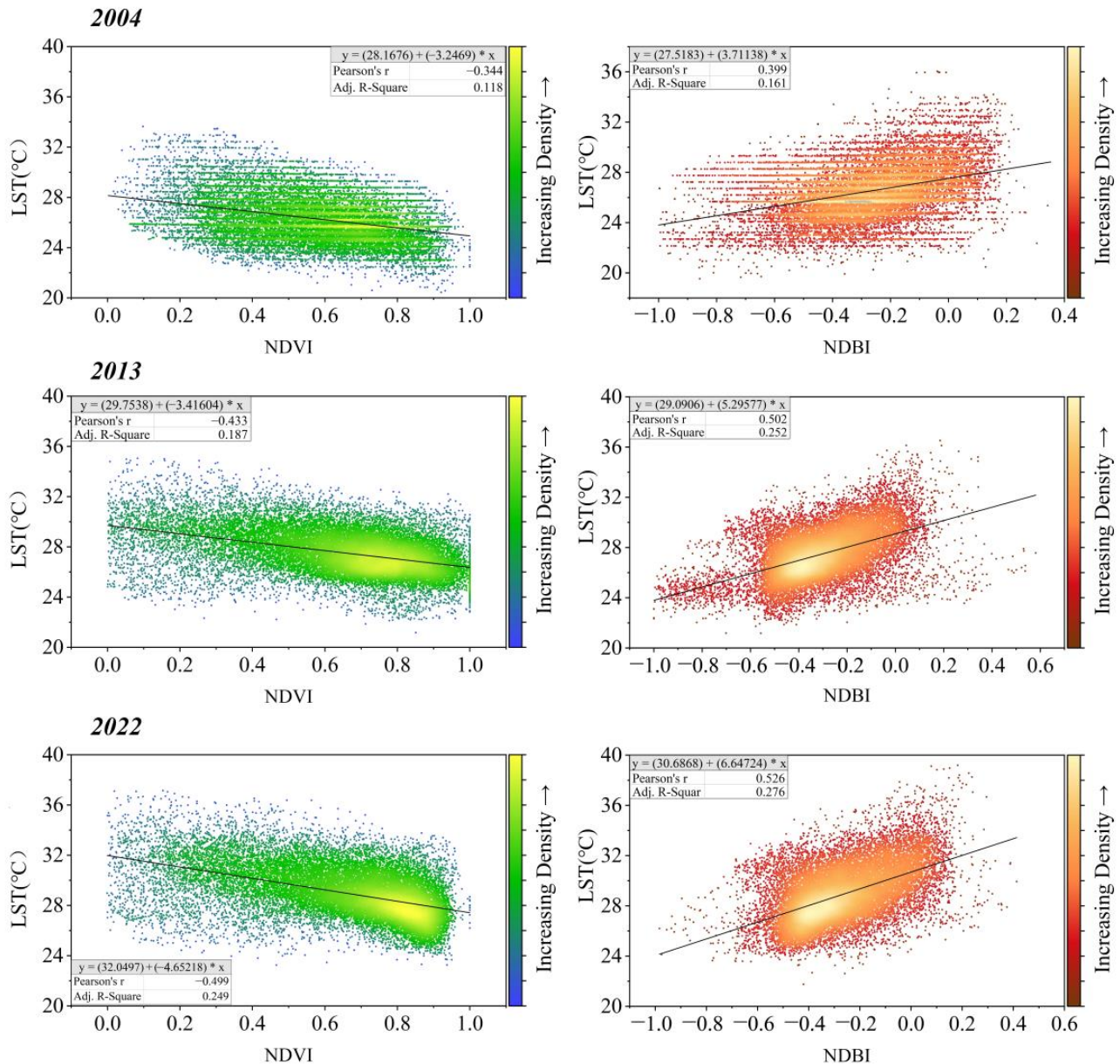


Figure 6. Correlation analysis between NDVI, NDBI, and LST.

Three indicators were linearly fitted to explain the influence of their changes on the LST of different land types. For every 0.1 increase in PLAND, VEG produced cooling rates of 0.16 °C, 0.20 °C, and 0.23 °C over three years, respectively. For CL, it caused a warming of 0.15 °C, 0.05 °C, and 0.12 °C. The warming degrees of IS were 0.29 °C, 0.36 °C, and 0.42 °C, whereas the cooling temperatures of WA were 0.42 °C, 0.38 °C, and 0.32 °C (Figure 8A). LPI had a similar trend as that of PLAND (Figure 8B). For every increase of 10 in DIVISION, the temperature effects of IS and WA become more dramatic, with the

former cooling by 0.38 °C, 0.45 °C, and 0.49 °C, respectively, in three years, and the latter warming by 0.47 °C, 0.44 °C, and 0.36 °C, respectively (Figure 8C).

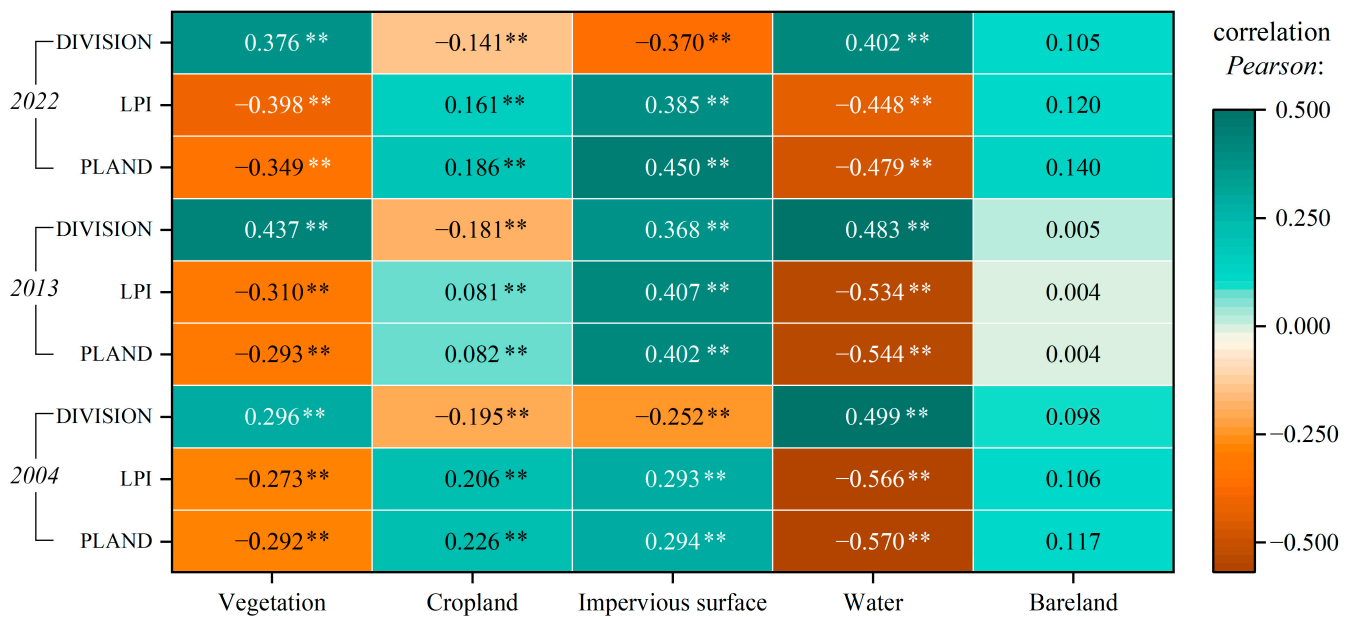


Figure 7. Correlation analysis between landscape indices and LST. ** Sig. level $p < 0.01$.

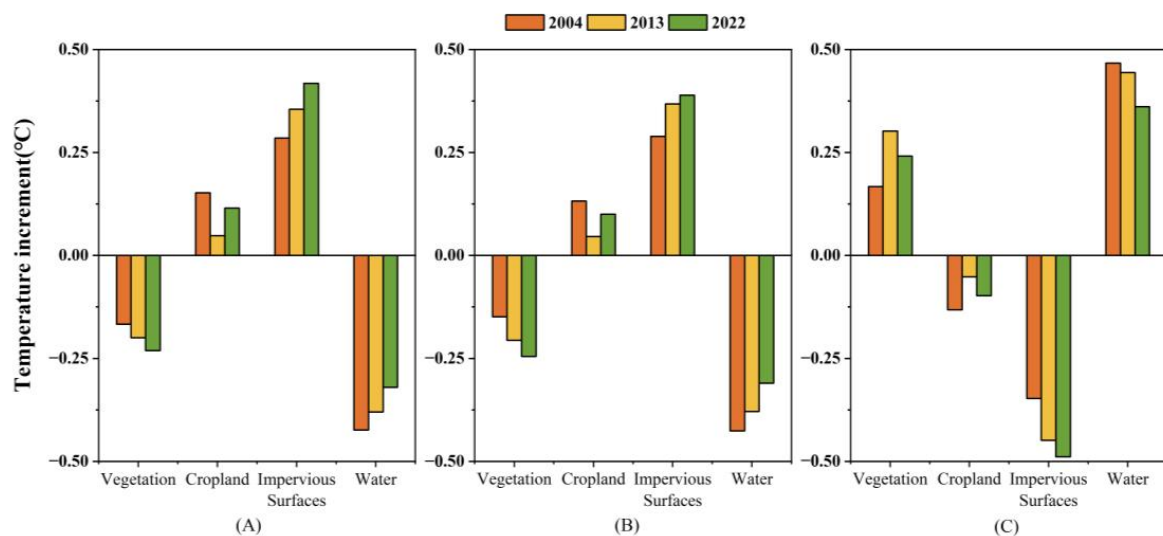


Figure 8. (A) Temperature change caused by PLAND for each rise of 0.1; (B) Temperature change caused by LPI for each rise of 0.1; (C) Temperature change caused by DIVISION for each rise of 10.

In summary, the impact of landscape indicators on IS and WA is higher than that of VEG and CL, with a rising influence in IS and a decreasing impact in WA. In addition to DIVISION, the impact of VEG is rising as well.

3.3. Analysis of the Impact of LUC Categories on LST

3.3.1. Average Temperature

The average temperatures of each land type are shown in Figure 9. Overall, the mean temperatures of IS were 27.33 °C, 29.21 °C, and 30.83 °C, respectively, making it the hottest land cover type in all years. Those of WA were 23.21 °C, 24.87 °C, and 26.52 °C, respectively, making it the coolest type. The average temperatures of CL were 26.58 °C, 27.55 °C, and 29.38 °C, while those of the vegetation were 25.63 °C, 27.20 °C, and 28.09 °C, respectively.

The average temperature of each land cover type increased remarkably during 2004–2013 and 2013–2022. From 2004 to 2013, the average temperature of the IS increased by 1.88 °C. From 2013 to 2022, the average temperature of BL increased by 2.37 °C, replacing IS as the type with the most substantial warming effect on land, while VEG had the least significant warming effect due to its cooling and humidifying properties, with a rise of only 0.86 °C.

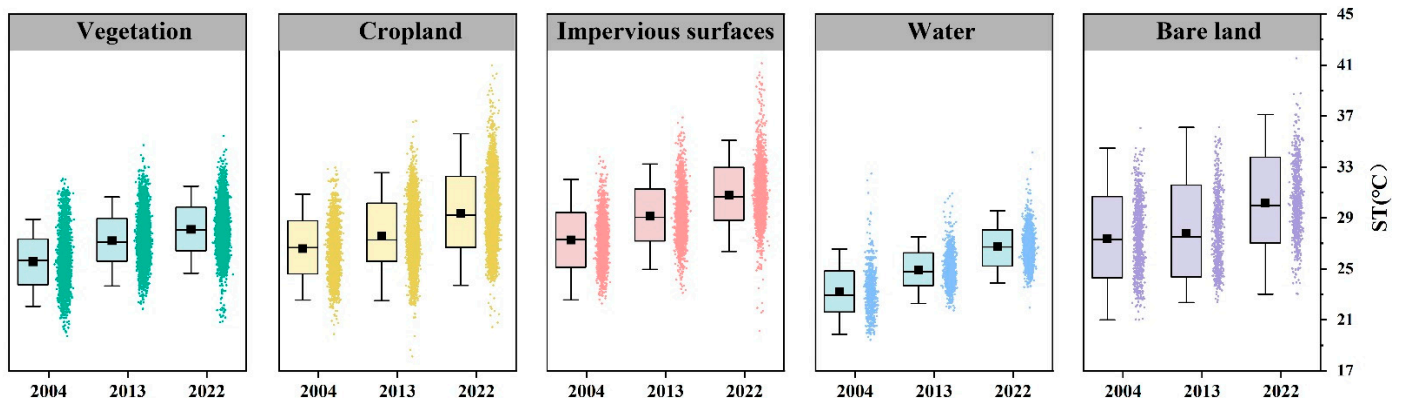


Figure 9. Average temperature of each land cover type in 2004, 2013, and 2022.

3.3.2. UTFVI Distribution

The UTFVI account for each land cover is shown in Figure 10. The strongest zones in CL, IS, and BL were relatively high, with the proportion in IS continuing to increase. The UTFVI area of CL decreased by about 17%, and the non-SUHI area rose. The non-SUHI was about 70%, with the strongest being about 16% of VEG. There were several SUHI in WA, accounting for only about 2%.

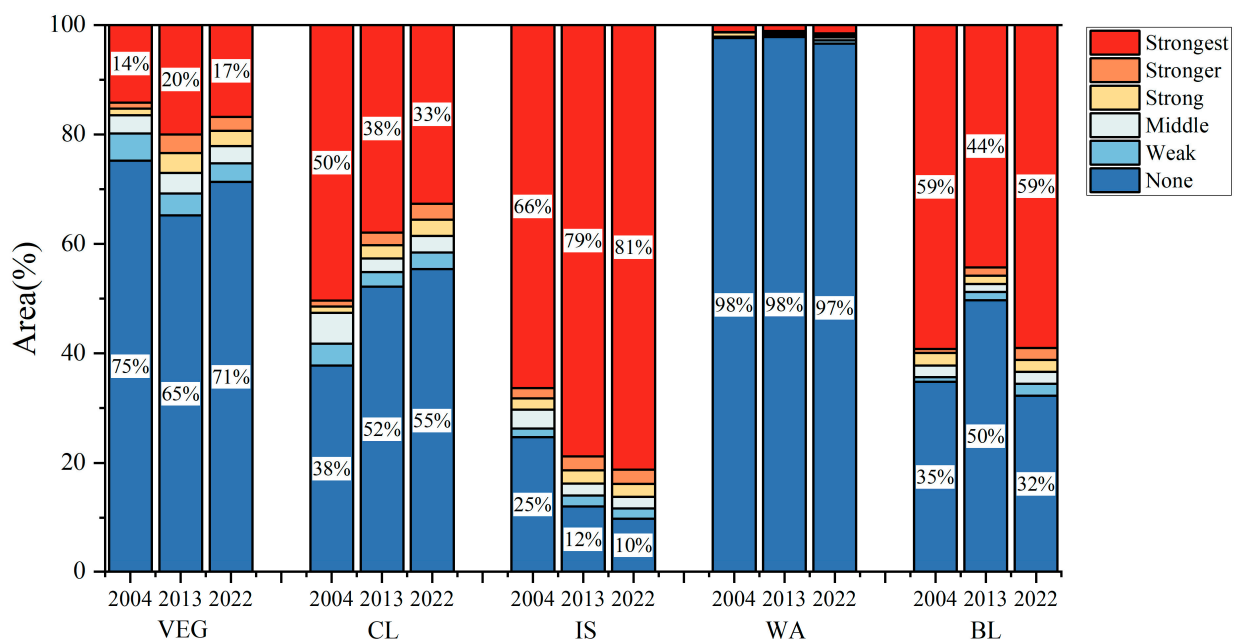


Figure 10. UTFVI accounts for each land cover.

3.3.3. Contribution of Different Land Cover to UTFVI

The UTFVI contribution over different land covers is evident in Figure 11. VEG was the dominant land of non-SUHI zones for all three years. UTFVI zone increased in IS from 9.33% in 2004 to 14.22% in 2022, whereas it decreased in CL from 21.26% in 2004 to 11.36% in 2022. From 2004 to 2013, CL recorded the strongest UTFVI zones. However, in

2022, IS recorded the most dominant UTFVI zones. This trend also existed in the strongest UTFVI areas.

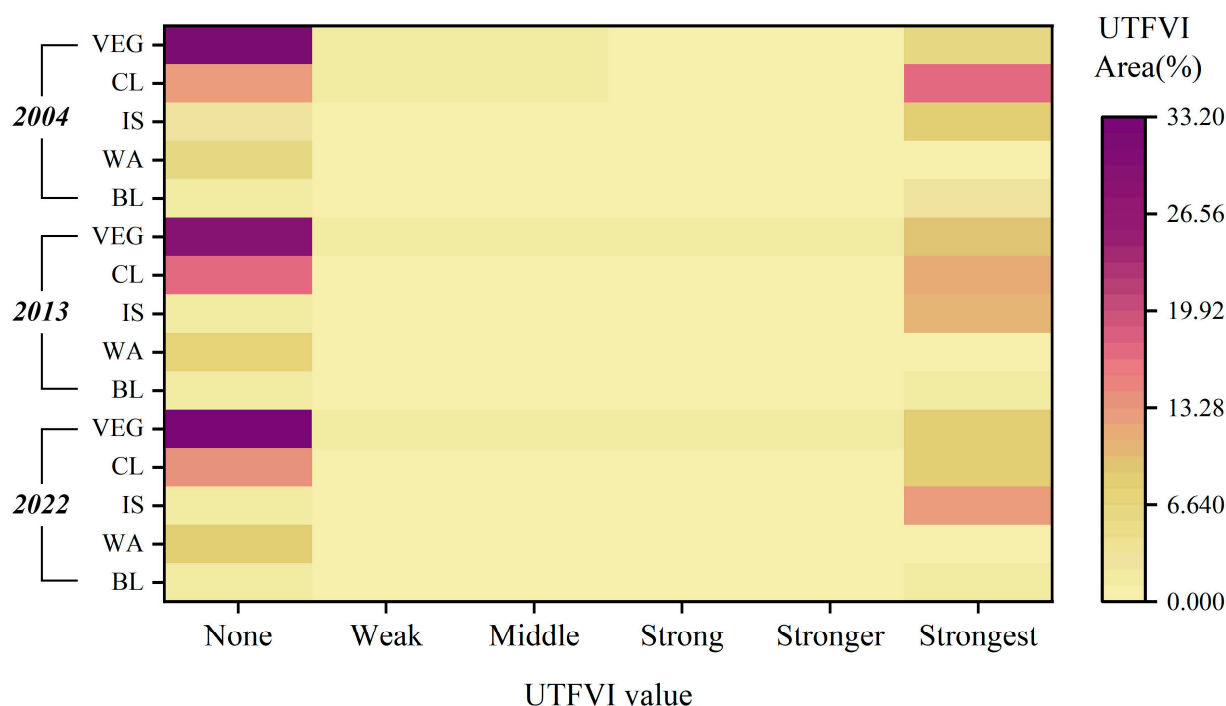


Figure 11. UTFVI contribution over different land covers.

4. Discussion

4.1. Land Cover and UHI Variation

During the period from 2004 to 2022, the land cover in Zhanjiang changed, primarily due to the growth of impervious surfaces and the loss of cropland. The spatial structure of Zhanjiang’s urban master plan (2011–2020) formed the overall spatial structure of Zhanjiang City. Based on the principles of “one Main and four Vice-centers, two Zones and two Axes”, which had a profound impact on the construction pattern changes in Zhanjiang. The central area of Zhanjiang is the zone with the greatest radiating power in the city, while Wuchuan, Leizhou, Lianjiang, and Xuwen counties are the sub-centers of Zhanjiang city that connect with the national strategic areas, whose land use patterns effectively respond to planning needs. Therefore, the impervious surface area of Zhanjiang has expanded outward from the center of “one Main and four Vice-centers” in the past 18 years. By 2022, we found that UHI zones almost entirely covered the impervious surfaces, indicating that urbanization is one of the important factors that aggravates the thermal environment of Zhanjiang.

Typically, vegetation, cropland, and water are the main cooling patches in the non-SUHI zones [30,47–49]. The study indicates that cropland is a thermal factor in Zhanjiang. Though the area of SUHI zones decreased from 62% to 45%, cropland’s average temperature rose by about 1.8 °C. The cause of the above phenomenon may be local volcanic soil, which has strong heat storage. Firstly, the surface thermal characteristics of the local volcanic soil, which has strong heat storage, are different from those of other cities [50]. A second factor contributing to the double growth in cropland area and planting density is the fertile soil and hydrothermal conditions that result in tropical fruits such as pineapple making up the largest portion of the local agricultural industry. Based on the General Land Use Plan for Zhanjiang, Guangdong (2006–2020), Zhanjiang currently faces the problems of poor agricultural production structures and low cropland efficiency. There is a proposal to promote intensive land transformation in Guangdong Province and establish a special agricultural base with a focus on agricultural land protection. Thus, under the orientation of thermal environment optimization, preserving the production value and quality of

cropland while mitigating thermal effects becomes a concern for agriculturally based cities. Urban planners should promote the comprehensive management of agricultural land, accounting for quantity, quality, and ecology. The use of green areas and water patches to meet cooling and humidification needs constitutes retrofit approaches for agricultural land with low production capacity.

The study results show that high-UTFVI areas are gradually concentrated in the IS area. However, due to the expansion of urban areas, the high-UTFVI areas of VEG and CL also have high proportions. The surface temperature was analyzed for the typical change areas of UTFVI for each type of land. (Figure 12). The Qingjianling vegetation area in Lianjiang is shown in Figure 12a. It was mostly covered by woodland in 2004 and showed an increase in impervious areas compared to 2022. The new cement company, garage, and funeral home are heavy burdens for the main SUHI areas, increasing the surrounding temperature of vegetation. Yugonglou village in Xuwen is shown in Figure 12b. Pineapple cultivation became the leading industry, raising economic needs such as agricultural production and transportation. Accordingly, both the area of cropland and the density of cultivation expanded, increasing the temperature of the cropland. The Baoshan Iron and Steel Factory in Ma Zhang District is shown in Figure 12c, which was an undeveloped coastal mudflat in 2004. Due to industrial production, it transformed almost all of it into impervious surfaces by 2022, with the SUHI zones growing accordingly. The Dashuiqiao Reservoir in Xuwen is shown in Figure 12d, where the water expanded between 2004 and 2012. The SUHI zones around the water grew due to the rising area of production teams, orchard farms, and residential land around the water. This led to the generation of SUHI areas and also affected the temperature of water surfaces.

The above indicates that, for less-developed cities similar to Zhanjiang, the increase in UTFVI is influenced not only by land cover type but also by population growth, the development of agricultural production, and the advancement of industrialization. Economic activities and resource allocation optimization have also become key social factors for the intensification of the urban heat island effect.

Impact of Land Cover Parameters

There is a significant negative correlation between the NDVI and LST, while the NDBI shows the opposite trend between 2004 and 2022. This indicates that conditions of vegetation cover cause temperature drops, while those of impervious surfaces cause temperature increases within $720\text{ m} \times 720\text{ m}$. The findings of this study are consistent with those of a number of previous studies [51–53]. NDVI and NDBI correlation coefficients increase to 0.499 and 0.526 in the study, which implies that vegetation provides greater cooling benefits and that impervious surfaces raise LST more for the same increase [54].

Even though the correlation coefficients between land cover parameters and LST are high, the fit R^2 scores of NDVI and NDBI are only 0.25 and 0.28, respectively, which illustrates that the number of units in the study area that could explain the correlation is low. Since the study is of a full-coverage area of the city with various and complex units, the south cropland influences the NDVI and NDBI fit with higher vegetation cover and lower building density but also presents a higher temperature, closely resembling the influence of land cover type on LST mentioned above. Compared to faster-developing cities, the influence mechanism of the thermal environment may be more complex, and land cover parameters cannot be considered as the single dominant factor of the thermal environment [29].

4.2. Impact of Landscape Pattern

According to the analysis of correlation coefficients of different landscape indices and LST, land cover parameters influence LST more than land cover patterns [34]. The fitting results indicate that vegetation, water bodies, and impervious surfaces are the three dominant land cover types affecting the thermal environment at the landscape pattern configuration level, which is consistent with the findings of Wu et al. [30]. Cropland's

pattern configuration data have improved in both correlation coefficients, but they remain low. Vegetation and water bodies exhibit negative correlations with PLAND, LPI, and DIVISION, whereas impervious surfaces exhibit positive correlations. The result is consistent with previous studies at both landscape and type levels [55,56].

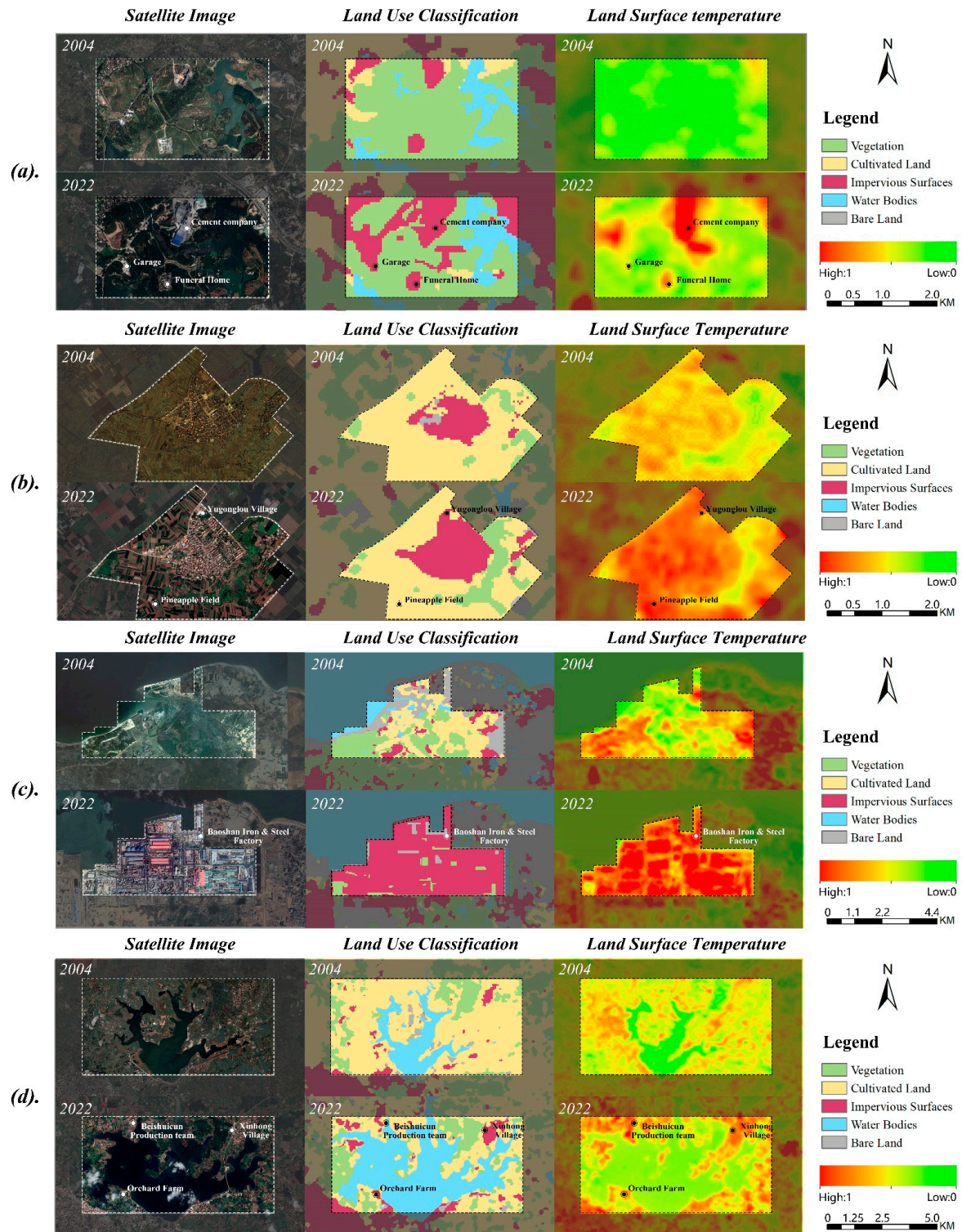


Figure 12. Satellite images, land use classification, and surface temperature for typical plots from 2004 to 2022. (a) Lianjiang City—Qingjianling; (b) Xuwen County—Yugonglou Village; (c) Ma Zhang District—Baoshan Iron and Steel Factory; (d) Xuwen County—Dashuiqiao Reservoir.

The Pearson correlation coefficient for impervious surfaces and water is higher in most cases. This suggests that impervious surfaces and water are the dominant types that affect LST at the landscape pattern level. Large areas of impervious materials, such as asphalt and concrete, can significantly increase LST [57], whereas water bodies play crucial roles in cooling temperature through evaporation [58,59], meaning that controlling the concentration of water and the dispersion of building surfaces is key. The landscape pattern index of vegetation and the Pearson correlation coefficient of LST show an overall upward trend. This means that large and concentrated green spaces will have more beneficial effects on Zhanjiang's thermal environment.

4.3. Suggestions for UHI Slowdown of Less-Developed Cities

The thermal environment of developing cities with relatively low levels of urbanization is also deteriorating [55], and it is a great challenge to balance urban economic development and environmental comfort. Through pixel-scale analysis, we demonstrated that changes in the types, parameters, and patterns of land cover in developing cities are all significantly correlated with the intensification of the UHI, suggesting that the disorderly expansion of impervious surfaces and the reduction and fragmentation of cooling patches will have an increasingly serious impact on the urban thermal environment in future developments. Therefore, it is necessary to provide urban development suggestions under the orientation of thermal environment optimization for developing cities that are accelerating their development. On the one hand, decision-makers should improve the quality of urban planning from the perspective of the management mode of land space to avoid the prolonged existence of ineffective land, such as "hollow cities" and "unused wasteland", which will affect the cooling benefits of the planned cooling patches for the cities. Conversely, it is necessary to implement the relevant national policies to support integrated and coordinated development, to pay attention to the protection of green areas and water bodies in the course of economic development, to strictly adhere to ecological red lines, and to control pollution emissions.

From the results of the study, NDVI and NDBI can to some extent indicate the temperature change in Zhanjiang City during the 18-year period; e.g., high-NDVI-value areas tend to imply extensive areas of green space, while impervious surfaces dominate the heat island in the center of the city where NDBI is higher. This implies that improving the vegetation cover and green quality of green spaces and habitats within the city is an important way to increase the cooling capacity of cooling patches in developing cities. For example, in future green public spaces and urban squares, trees with high canopy covers can be selected to increase vegetation cover and provide good shading and cooling. Additionally, the layout and planning of blue-green spaces are crucial to the planning of developing cities. Urban planners need to pay attention not only to increasing the landscape percentage of the landscape (PLAND) but also to raising the size of the maximum patch index (LPI) and decreasing the separation between patches (DIVISION) when coordinating blue-green space. In the case of impervious surfaces, cropland, partially abandoned cropland, and bare land, replanting trees between impervious surfaces and cropland would create a greener system with improved cooling and reduced fragmentation. By improving lake wind circulation [60], water surface heating promotes heat outflow within the urban canopy. To maximize cooling benefits, vegetation should complement the perimeter of water bodies, allowing the maximization of cooling benefits. To avoid urban sprawl sequentially, the degree of separation between buildings (DIVISION) needs to be increased, implying that the continuous expansion of impervious surfaces should be controlled and that future urban site planning should be decentralized properly. Additionally, the degree of intensification of construction areas should be improved, transforming idle and inefficient construction land into urban public green space to enhance the regulation function of the urban ecosystem on the thermal environment and create an urban living space with people-oriented and healthy development.

4.4. Limitations and Prospects

The present study has certain limitations. Firstly, previous research has indicated that the correlation between landscape indices and land surface temperature (LST) can be influenced by grid scales and seasonal variations [61,62]. In the case of Zhanjiang, the geographical location and municipal boundaries make the rural–urban gradient method less applicable for studying the thermal environment. Future studies could explore different grid sizes in graded urban and rural areas to determine the most suitable study cell size for each area.

Secondly, the utilization of open-source satellite imagery offers convenient access to long-time series images and valuable waveform information, which can be utilized to predict sustainable land use, ecosystem management, and climate change [17]. However, due to the study area being situated in a humid tropical region with significant cloud pollution, the availability of satellite images suitable for interpretation is limited. As a result, this study could only reveal the correlation between land cover information and LST during the daytime in the autumn for the observed years. In future studies, we should try to collect all available images in a month or a season and integrate the LSTs of the calculation region to enhance the convincing power of the data and conclusions.

Finally, the thermal environment of the land cover is influenced by multiple factors, and the parameters and patterns utilized in this study exhibit lower fit and correlation coefficients with LST compared to most existing literature. This indicates the need for a more comprehensive evaluation system of the thermal environment in future studies, which should incorporate natural factors such as topography and integrate more data sources along with human factors such as economic development.

5. Conclusions

This study examines the relationship between changes in land cover and the thermal environment in Zhanjiang from 2004 to 2022. The focus is on investigating the correlation between spatiotemporal variations in land cover parameters, specifically NDVI (normalized difference vegetation index) and NDBI (normalized difference built-up index), and three landscape pattern indices—PLAND, LPI, and DIVISION. The ultimate goal is to propose effective strategies for mitigating the thermal environment in Zhanjiang. The key findings and conclusions of this study are as follows:

1. Over the past 18 years, the thermal conditions in Zhanjiang have become more intense. This is reflected in a significant increase in the average temperature of the heat island and non-heat island regions in relation to UTFVI. The urban thermal field generally showed a trend of expansion to the north and northwest.
2. LST (land surface temperature) is strongly linked to land cover parameters, exhibiting a negative correlation with NDVI and a positive correlation with NDBI. For every 0.1 increase in NDVI, the overall LST is reduced by approximately 0.32–0.47 °C. Conversely, in the case of NDBI, this increases by about 0.37–0.67 °C. Correlation coefficients and the analysis of the fit indicate that the warming effect of NDBI outweighs the cooling effect of NDVI.
3. Correlation analysis reveals that the landscape pattern index at the type level is strongly associated with land surface temperature (LST). The percentage of land cover (PLAND) and the landscape shape index (LPI) of vegetation and water bodies are negatively correlated with LST, meaning they contribute to cooling. On the other hand, the DIVISION index shows a positive correlation with LST, indicating a warming effect, which is true for cropland and impervious surfaces. Among these factors, the DIVISION index has the most significant impact on LST.
4. Impervious surfaces and cropland play important roles in the intensification of the thermal field in Zhanjiang, but the impact of cropland is generally decreasing, and the impervious surfaces have gradually come to dominate the UHI. The UHI of water accounts for only about 2% of the total. However, due to the low proportion of such

areas, vegetation still dominates non-UHI areas. In addition, due to the wide coverage, vegetation also makes an overall contribution of about 10% to the UHI.

This study focuses on the spatiotemporal development of the urban thermal environment and the linkage between the changes in the land cover to provide experience and reference for future urban landscape layout and land use planning with thermal environment mitigation as the focus.

Author Contributions: Conceptualization, Y.H. and D.L.; methodology, Y.H. and H.L.; software, Y.H. and H.L.; validation, Y.H., H.L. and D.L.; formal analysis, Y.H.; investigation, M.A.S. and Y.H.; resources, M.A.S. and D.L.; data curation, Y.H. and H.L.; writing—original draft preparation, Y.H.; writing—review and editing, Y.H.; visualization, H.L.; supervision, D.L. All authors have read and agreed to the published version of the manuscript.

Funding: This research received no external funding.

Institutional Review Board Statement: Not applicable.

Informed Consent Statement: Not applicable.

Data Availability Statement: The data presented in this study are available upon request from the corresponding author.

Conflicts of Interest: The authors declare no conflict of interest.

References

1. Hassan, T.; Zhang, J.; Proadhan, F.A.; Pangali Sharma, T.P.; Bashir, B. Surface urban heat islands dynamics in response to LULC and vegetation across South Asia (2000–2019). *Remote Sens.* **2021**, *13*, 3177. [[CrossRef](#)]
2. Rinner, C.; Hussain, M. Toronto's urban heat island—Exploring the relationship between land use and surface temperature. *Remote Sens.* **2011**, *3*, 1251–1265. [[CrossRef](#)]
3. Owen, T.W.; Carlson, T.N.; Gillies, R.R. An assessment of satellite remotely-sensed land cover parameters in quantitatively describing the climatic effect of urbanization. *Int. J. Remote Sens.* **2010**, *19*, 1663–1681. [[CrossRef](#)]
4. Pal, S.; Ziaul, S. Detection of land use and land cover change and land surface temperature in English Bazar urban centre. *Egypt. J. Remote Sens. Space Sci.* **2017**, *20*, 125–145. [[CrossRef](#)]
5. Voogt, J.A.; Oke, T.R. Thermal remote sensing of urban climates. *Remote Sens. Environ.* **2003**, *86*, 370–384. [[CrossRef](#)]
6. Yu, Y.; Li, J.; Zhu, C.; Plaza, A. Urban Impervious Surface Estimation from Remote Sensing and Social Data. *Photogramm. Eng. Remote Sens.* **2018**, *84*, 771–780. [[CrossRef](#)]
7. Santamouris, M.; Cartalis, C.; Synnefa, A.; Kolokotsa, D. On the impact of urban heat island and global warming on the power demand and electricity consumption of buildings—A review. *Energ. Build.* **2015**, *98*, 119–124. [[CrossRef](#)]
8. Huang, H.; Yang, H.; Chen, Y.; Chen, T.; Bai, L.; Peng, Z. Urban green space optimization based on a climate health risk appraisal—A case study of Beijing city, China. *Urban For. Urban Green.* **2021**, *62*, 127154. [[CrossRef](#)]
9. Noelke, C.; McGovern, M.; Corsi, D.J.; Jimenez, M.P.; Stern, A.; Wing, I.S.; Berkman, L. Increasing ambient temperature reduces emotional well-being. *Environ. Res.* **2016**, *151*, 124–129. [[CrossRef](#)]
10. Li, X.; Zhou, W.; Ouyang, Z.; Xu, W.; Zheng, H. Spatial pattern of greenspace affects land surface temperature: Evidence from the heavily urbanized Beijing metropolitan area, China. *Landsc. Ecol.* **2012**, *27*, 887–898. [[CrossRef](#)]
11. Estoque, R.C.; Murayama, Y.; Myint, S.W. Effects of landscape composition and pattern on land surface temperature: An urban heat island study in the megacities of Southeast Asia. *Sci. Total Environ.* **2017**, *577*, 349–359. [[CrossRef](#)] [[PubMed](#)]
12. Shen, C.; Hou, H.; Zheng, Y.; Murayama, Y.; Wang, R.; Hu, T. Prediction of the future urban heat island intensity and distribution based on landscape composition and configuration: A case study in Hangzhou. *Sustain. Cities Soc.* **2022**, *83*, 103992. [[CrossRef](#)]
13. Li, Y.; Liu, Y.; Ranagalage, M.; Zhang, H.; Zhou, R. Examining land use/land cover change and the summertime surface urban heat island effect in fast-growing Greater Hefei, China: Implications for sustainable land development. *SPRS Int. J. Geo-Inf.* **2020**, *9*, 568. [[CrossRef](#)]
14. Dai, Z.; Guldman, J.; Hu, Y. Spatial regression models of park and land-use impacts on the urban heat island in central Beijing. *Sci. Total Environ.* **2018**, *626*, 1136–1147. [[CrossRef](#)] [[PubMed](#)]
15. Chen, X.; Zhang, Y. Impacts of urban surface characteristics on spatiotemporal pattern of land surface temperature in Kunming of China. *Sustain. Cities Soc.* **2017**, *32*, 87–99. [[CrossRef](#)]
16. Chen, H.; Deng, Q.; Zhou, Z.; Ren, Z.; Shan, X. Influence of land cover change on spatio-temporal distribution of urban heat island—A case in Wuhan main urban area. *Sustain. Cities Soc.* **2022**, *79*, 103715. [[CrossRef](#)]
17. Wang, R.; Hou, H.; Murayama, Y.; Dourdour, A. Spatiotemporal analysis of land use/cover patterns and their relationship with land surface temperature in Nanjing, China. *Remote Sens.* **2020**, *12*, 440. [[CrossRef](#)]

18. Wang, H.; Zhang, Y.; Tsou, J.; Li, Y. Surface urban heat island analysis of Shanghai (China) based on the change of land use and land cover. *Sustainability* **2017**, *9*, 1538. [[CrossRef](#)]
19. Xiong, Y.; Huang, S.; Chen, F.; Ye, H.; Wang, C.; Zhu, C. The impacts of rapid urbanization on the thermal environment: A remote sensing study of Guangzhou, South China. *Remote Sens.* **2012**, *4*, 2033–2056. [[CrossRef](#)]
20. Li, W.; Bai, Y.; Chen, Q.; He, K.; Ji, X.; Han, C. Discrepant impacts of land use and land cover on urban heat islands: A case study of Shanghai, China. *Ecol. Indic.* **2014**, *47*, 171–178. [[CrossRef](#)]
21. Yu, W.; Shi, J.; Fang, Y.; Xiang, A.; Li, X.; Hu, C.; Ma, M. Exploration of urbanization characteristics and their effect on the urban thermal environment in Chengdu, China. *Build. Environ.* **2022**, *219*, 109150. [[CrossRef](#)]
22. Du, C.; Song, P.; Wang, K.; Li, A.; Hu, Y.; Zhang, K.; Jia, X.; Feng, Y.; Wu, M.; Qu, K.; et al. Investigating the trends and drivers between urbanization and the land surface temperature: A case study of Zhengzhou, China. *Sustainability* **2022**, *14*, 13845. [[CrossRef](#)]
23. Du, S.; Xiong, Z.; Wang, Y.; Guo, L. Quantifying the multilevel effects of landscape composition and configuration on land surface temperature. *Remote Sens. Environ.* **2016**, *178*, 84–92. [[CrossRef](#)]
24. Hou, H.; Estoque, R.C. Detecting cooling effect of landscape from composition and configuration: An urban heat island study on Hangzhou. *Urban For. Urban Green.* **2020**, *53*, 126719. [[CrossRef](#)]
25. Peng, J.; Hu, Y.; Dong, J.; Liu, Q.; Liu, Q. Quantifying spatial morphology and connectivity of urban heat islands in a megacity: A radius approach. *Sci. Total Environ.* **2020**, *714*, 136792. [[CrossRef](#)] [[PubMed](#)]
26. Hamoodi, M.N.; Corner, R.; Dewan, A. Thermophysical behaviour of LULC surfaces and their effect on the urban thermal environment. *J. Spat. Sci.* **2019**, *64*, 111–130. [[CrossRef](#)]
27. Duncan, J.M.A.; Boruff, B.; Saunders, A.; Sun, Q.; Hurley, J.; Amati, M. Turning down the heat: An enhanced understanding of the relationship between urban vegetation and surface temperature at the city scale. *Sci. Total Environ.* **2019**, *656*, 118–128. [[CrossRef](#)] [[PubMed](#)]
28. Wu, Q.; Tan, J.; Guo, F.; Li, H.; Chen, S. Multi-scale relationship between land surface temperature and landscape pattern based on Wavelet Coherence: The case of Metropolitan Beijing, China. *Remote Sens.* **2019**, *11*, 3021. [[CrossRef](#)]
29. Liu, S.; Li, X.; Chen, L.; Zhao, Q.; Zhao, C.; Hu, X.; Li, J. A new approach to investigate the spatially heterogeneous in the cooling effects of landscape pattern. *Land* **2022**, *11*, 239. [[CrossRef](#)]
30. Wu, Y.; Hou, H.; Wang, R.; Murayama, Y.; Wang, L.; Hu, T. Effects of landscape patterns on the morphological evolution of surface urban heat island in Hangzhou during 2000–2020. *Sustain. Cities Soc.* **2022**, *79*, 103717. [[CrossRef](#)]
31. Estoque, R.C.; Murayama, Y. Monitoring surface urban heat island formation in a tropical mountain city using Landsat data (1987–2015). *ISPRS J. Photogramm.* **2017**, *133*, 18–29. [[CrossRef](#)]
32. Wu, Z.; Zhang, Y. Spatial variation of urban thermal environment and its relation to green space patterns: Implication to sustainable landscape planning. *Sustainability* **2018**, *10*, 2249. [[CrossRef](#)]
33. Athukorala, D.; Murayama, Y. Spatial variation of land use/cover composition and impact on surface urban heat island in a tropical sub-Saharan city of Accra, Ghana. *Sustainability* **2020**, *12*, 7953. [[CrossRef](#)]
34. Wang, L.; Hou, H.; Weng, J. Ordinary least squares modelling of urban heat island intensity based on landscape composition and configuration: A comparative study among three megacities along the Yangtze River. *Sustain. Cities Soc.* **2020**, *62*, 102381. [[CrossRef](#)]
35. Zhou, W.; Cao, F. Effects of changing spatial extent on the relationship between urban forest patterns and land surface temperature. *Ecol. Indic.* **2020**, *109*, 105778. [[CrossRef](#)]
36. Anees, M.M.; Mann, D.; Sharma, M.; Banzhaf, E.; Joshi, P.K. Assessment of Urban Dynamics to Understand Spatiotemporal Differentiation at Various Scales Using Remote Sensing and Geospatial Tools. *Remote Sens.* **2020**, *12*, 1306. [[CrossRef](#)]
37. Song, J.; Du, S.; Feng, X.; Guo, L. The relationships between landscape compositions and land surface temperature: Quantifying their resolution sensitivity with spatial regression models. *Landsc. Urban Plan.* **2014**, *123*, 145–157. [[CrossRef](#)]
38. Sobrino, J.A.; Jiménez-Muñoz, J.C.; Paolini, L. Land surface temperature retrieval from Landsat TM 5. *Remote Sens. Environ.* **2004**, *90*, 434–440. [[CrossRef](#)]
39. Chander, G.; Markham, B.L.; Helder, D.L. Summary of current radiometric calibration coefficients for Landsat MSS, TM, ETM+, and EO-1 ALI sensors. *Remote Sens. Environ.* **2009**, *113*, 893–903. [[CrossRef](#)]
40. Malaret, E.; Bartolucci, L.; Lozano, D.; Antlta, P.; McGillem, C. Landsat-4 and Landsat-5 thematic mapper data quality analysis. *Photogramm. Eng. Remote Sens.* **1985**, *51*, 1407–1416.
41. Barsi, J.; Schott, J.; Hook, S.; Raqueno, N.; Markham, B.; Radocinski, R. Landsat-8 thermal infrared sensor (TIRS) vicarious radiometric calibration. *Remote Sens.* **2014**, *6*, 11607–11626. [[CrossRef](#)]
42. Arabi Aliabad, F.; Zare, M.; Ghafarian Malamiri, H. Comparison of the accuracy of daytime land surface temperature retrieval methods using Landsat 8 images in arid regions. *Infrared Phys Techn.* **2021**, *115*, 103692. [[CrossRef](#)]
43. Silvestri, M.; Rabuffi, F.; Pisciotta, A.; Musacchio, M.; Diliberto, I.S.; Spinetti, C.; Lombardo, V.; Colini, L.; Buongiorno, M.F. Analysis of thermal anomalies in volcanic areas using multiscale and multitemporal monitoring; Vulcano Island test case. *Remote Sens.* **2019**, *11*, 134. [[CrossRef](#)]
44. Hua, L.; Wang, H.; Zhang, H.; Sun, F.; Li, L.; Tang, L. A new technique for impervious surface mapping and its spatio-temporal changes from Landsat and Sentinel-2 images. *Sustainability* **2023**, *15*, 7947. [[CrossRef](#)]

45. Hidalgo-García, D.; Arco-Díaz, J. Modeling the surface urban heat island (SUHI) to study of its relationship with variations in the thermal field and with the indices of land use in the metropolitan area of Granada (Spain). *Sustain. Cities Soc.* **2022**, *87*, 104166. [[CrossRef](#)]
46. Anderson, J.R. Land use classification schemes used in selected recent geographic applications of remote sensing. *Photogramm. Eng.* **1971**, *37*, 379–387.
47. Saha, S.; Saha, A.; Das, M.; Saha, A.; Sarkar, R.; Das, A. Analyzing spatial relationship between land use/land cover (LULC) and land surface temperature (LST) of three urban agglomerations (UAs) of Eastern India. *Remote Sens. Appl. Soc. Environ.* **2021**, *22*, 100507. [[CrossRef](#)]
48. Khan, M.S.; Ullah, S.; Chen, L. Comparison on land-use/land-cover indices in explaining land surface temperature variations in the city of Beijing, China. *Land* **2021**, *10*, 1018. [[CrossRef](#)]
49. Fonseka, H.P.U.; Zhang, H.; Sun, Y.; Su, H.; Lin, H.; Lin, Y. Urbanization and its impacts on land surface temperature in Colombo Metropolitan Area, Sri Lanka, from 1988 to 2016. *Remote Sens.* **2019**, *11*, 957. [[CrossRef](#)]
50. Lane, P.N.J.; Morris, J.; Ningnan, Z.; Guangyi, Z.; Guoyi, Z.; Daping, X. Water balance of tropical eucalypt plantations in south-eastern China. *Agric. For. Meteorol.* **2004**, *124*, 253–267. [[CrossRef](#)]
51. Rashid, N.; Alam, J.A.M.M.; Chowdhury, M.A.; Islam, S.L.U. Impact of landuse change and urbanization on urban heat island effect in Narayanganj city, Bangladesh: A remote sensing-based estimation. *Environ. Chall.* **2022**, *8*, 100571. [[CrossRef](#)]
52. Sekertekin, A.; Zadbagher, E. Simulation of future land surface temperature distribution and evaluating surface urban heat island based on impervious surface area. *Ecol. Indic.* **2021**, *122*, 107230. [[CrossRef](#)]
53. Silva, A.G.L.; Torres, M.C.A. Proposing an effective and inexpensive tool to detect urban surface temperature changes associated with urbanization processes in small cities. *Build. Environ.* **2021**, *192*, 107634. [[CrossRef](#)]
54. Sun, Z.; Li, Z.; Zhong, J. Analysis of the impact of landscape patterns on urban heat islands: A case study of Chengdu, China. *Int. J. Environ. Res. Public Health* **2022**, *19*, 13297. [[CrossRef](#)]
55. Zhang, Y.; Wang, Y.; Ding, N.; Yang, X. Spatial pattern impact of impervious surface density on urban heat island effect: A case study in Xuzhou, China. *Land* **2022**, *11*, 2135. [[CrossRef](#)]
56. Azhdari, A.; Soltani, A.; Alidadi, M. Urban morphology and landscape structure effect on land surface temperature: Evidence from Shiraz, a semi-arid city. *Sustain. Cities Soc.* **2018**, *41*, 853–864. [[CrossRef](#)]
57. Portela, C.I.; Massi, K.G.; Rodrigues, T.; Alcântara, E. Impact of urban and industrial features on land surface temperature: Evidences from satellite thermal indices. *Sustain. Cities Soc.* **2020**, *56*, 102100. [[CrossRef](#)]
58. Tariq, A.; Mumtaz, F. Modeling spatio-temporal assessment of land use land cover of Lahore and its impact on land surface temperature using multi-spectral remote sensing data. *Environ. Sci. Pollut. Res. Int.* **2023**, *30*, 23908–23924. [[CrossRef](#)] [[PubMed](#)]
59. Amir Siddique, M.; Boqing, F.; Dongyun, L. Modeling the impact and risk assessment of urbanization on urban heat island and thermal comfort level of Beijing City, China (2005–2020). *Sustainability* **2023**, *15*, 6043. [[CrossRef](#)]
60. Zhu, D.; Zhou, X.; Cheng, W. Water effects on urban heat islands in summer using WRF-UCM with gridded urban canopy parameters—A case study of Wuhan. *Build. Environ.* **2022**, *225*, 109528. [[CrossRef](#)]
61. Guo, L.; Liu, R.; Men, C.; Wang, Q.; Miao, Y.; Zhang, Y. Quantifying and simulating landscape composition and pattern impacts on land surface temperature: A decadal study of the rapidly urbanizing city of Beijing, China. *Sci. Total Environ.* **2019**, *654*, 430–440. [[CrossRef](#)] [[PubMed](#)]
62. Chen, Y.; Yang, J.; Yu, W.; Ren, J.; Xiao, X.; Xia, J.C. Relationship between urban spatial form and seasonal land surface temperature under different grid scales. *Sustain. Cities Soc.* **2023**, *89*, 104374. [[CrossRef](#)]

Disclaimer/Publisher’s Note: The statements, opinions and data contained in all publications are solely those of the individual author(s) and contributor(s) and not of MDPI and/or the editor(s). MDPI and/or the editor(s) disclaim responsibility for any injury to people or property resulting from any ideas, methods, instructions or products referred to in the content.